Design Rule and Orientation Layout for MEMS Curved Beams on Silicon

Tzung-Ming Chen, Zhenyu Liu, Jan G. Korvink, and Ulrike Wallrabe

***Abstract*—An analysis method used to choose a suitable structural orientation layout for a microcompliant mechanism, which includes multi-curved-beams, is introduced, particularly, for fabricating microelectromechanical-systems (MEMS) thin-curved-beam microstructures on (100) and (111) single-crystal silicon (SCS) wafers. The achievement of a large deflection of a fabricated SCS device verifies the usability of this design rule. The orientation layouts of the device for a large deflection are restricted to a specific region. Based on the analysis method, it is better to follow a 21° safe region between the ⟨100⟩ and ⟨110⟩ orientations in order to decrease the possibility of crystal slip failure. Using this design consideration, one can design more robust MEMS compliant mechanisms from SCS, exploiting its ideal elasticity. [2009-0149]**

***Index Terms*—Compliant mechanism, large deflection, single-crystal silicon (SCS), stiffness matrix.**

I. Introduction

SINGLE-CRYSTAL silicon (SCS) is an anisotropic and brittle material with a high Young's modulus. It is one of the most used materials in microelectromechanical systems (MEMS). Many different SCS microdevices can be developed by using compliant mechanisms to achieve the elastic and kinematic functions [1]. This kind of microdevice uses the deflection of the structure to fulfill a specific motion. A successful compliant mechanism has many advantages, for example, it simplifies the manufacturing and assembly procedure, maintains a precise kinematic path and avoids friction in motion [2], and smoothens the stress distribution. The main design goal for compliant mechanisms is the reliability of the mechanism [3]. Compared to static structures, it is much more important for compliant mechanisms to achieve reliability of a kinematic motion through a sophisticated design [4]. For this reason, the relation between the material properties and the reliability of a micro-SCS kinematic mechanism has to be discussed.

In the design procedure, the structural topology is one of the primary factors that need to be considered. The big challenge for a designer is how to obtain an optimized mechanism and simplify a complicated structural topology in order to satisfy a precise kinematic motion and balance the stiffness and compliance in order to maintain the elastic deformation of SCS. Based on the directional Young's modulus of SCS, it is necessary to assign a motion range of a device and predict the behavior limit, which is also a design objective. Therefore, Young's modulus and the fracture strength of SCS need to be considered and treated as the design constraints. Relying on these two parameters, the spring constant and the structural topology are able to reinforce each other. Furthermore, in order to obtain a smooth structural profile and overcome stress problems, a new design concept with curved beams is used. A curved-beam design is more efficient than a traditional straight-beam design for a large deflection application because both of stress concentrations and nonsmooth distributions of stress are easier to be handled in a curved beam [5].

However, a single-crystal structure does not have the grain boundary strengthening mechanism because of its atomic arrangement. When the material is actuated by an external force, crystal slip easily happens in this kind of materials due to shear stress. Normally, the theoretical fracture strength of a single-crystal material is 100 times higher than the critical resolved shear stress which follows the slip direction of the material [6], [7]. Therefore, a safe region on an SCS wafer has to be defined in order to avoid or decrease the possibility of stress-induced crystal slip. Based on the consideration, the calculation of the stiffness can be trusted, and the decision of the mechanical safety factor is then reliable. This means that the theoretical elasticity of the SCS can be exploited. This is the reason why we focus on the relation of the anisotropy and the orientation layout of an SCS compliant mechanism, particularly with a large deflection. In other words, orientation layout is an important consideration to maintain the kinematic robustness before an SCS compliant mechanism has been fabricated. If this consideration is missed, the given function of a device that was decided in the design stage would be limited.

Based on basic theories, correct analysis, and suitable simulation tools, we can predict the feasibility of fabrication and the capability of a product and save time to obtain a successful product. The corresponding stiffness in the ⟨100⟩, ⟨110⟩, and ⟨111⟩ orientations can be calculated by a generalized Hooke's law by means of Young's modulus, shear modulus, and Poisson's ratio [8], [9]. By using a transformation tensor,

Manuscript received June 9, 2009; revised February 6, 2010; accepted March 18, 2010. Date of publication May 10, 2010; date of current version June 3, 2010. Subject Editor D.-I. Cho.

T.-M. Chen was with the Laboratory for Microactuators, Department of Microsystems Engineering (IMTEK), University of Freiburg, 79110 Freiburg, Germany. He is now with the Department of Mechanical Engineering, Army Academy, Jhongli City 320, Taiwan (e-mail: tm@mnst.tw).

Z. Liu was with the Laboratory for Simulation, IMTEK, University of Freiburg, 79110 Freiburg, Germany. He is now with Changchun Institute of Optics, Fine Mechanics and Physics, Chinese Academy of Sciences, Changchun 130033, China.

J. G. Korvink is with the Laboratory for Simulation, IMTEK, University of Freiburg, 79110 Freiburg, Germany, and also with the Freiburg Institute of Advanced Studies (FRIAS), University of Freiburg, 79104 Freiburg, Germany.

U. Wallrabe is with the Laboratory for Microactuators, IMTEK, University of Freiburg, 79110 Freiburg, Germany, and also with FRIAS, University of Freiburg, 79104 Freiburg, Germany.

Color versions of one or more of the figures in this paper are available online at http://ieeexplore.ieee.org.

Digital Object Identifier 10.1109/JMEMS.2010.2048416

TABLE I
SPECIFIC OUTPUT DISPLACEMENT IN THE Y-DIRECTION IN A CONSTRAINED DESIGN AREA IS THE DESIGN OBJECTIVE. THE CURVED BEAM SHOWS A HIGHER POSSIBILITY TO ACHIEVE THE OBJECTIVE WITH A LOWER STRESS AND EXTERNAL FORCE

Specification		
Design area: 200 μm× 100 μm Beam thickness: 20 μm Beam length: 200 μm Fix position: Left side	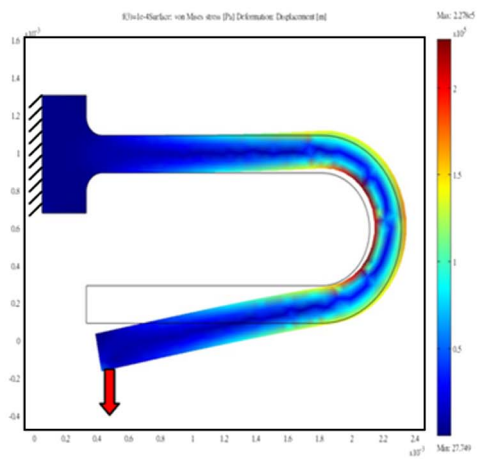	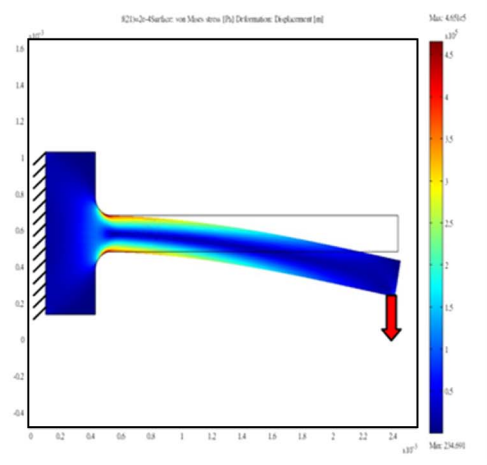
Output displacement	42 μm	41.5 μm
Max. stress	227 kPa	465 kPa
External force	0.1 mN	0.2 mN

the stiffness of any specific orientation can be mapped [10]. For example, if one straight beam is planned to be actuated in a simple bending mode with a small deflection, it is not a big issue to lay the beam on an SCS wafer in order to avoid the orientation of the maximum shear stress to align with the $\langle 110 \rangle$ direction. In this kind of situation, relying on the transformation tensor, the mechanical behavior of the beam can be predicted. Nevertheless, the orientation layout of a multi-curved-beam compliant mechanism could not rely only on a generalized Hooke's law. Because of the change of the stress state during the actuation, the balance among the actuation direction, the anisotropy properties, and the structural topology has to be solved "case by case." By using "trial and error" to find a suitable orientation often wastes more time and cost. In other words, a specific analysis of safe region on an SCS wafer for different structural profiles and different loading modes is necessary.

Therefore, in this paper, an in-plane rotational mirror [11] is used as an example to discuss the calculation and analysis process, as well as to determine a useful criterion for orientation layout of thin-beam structures. Furthermore, in order to achieve a large deflection and maintain the reliability, a suitable orientation layout on an SCS wafer has to be chosen to decrease the possibility of crystal slip failure during kinematic motion. At the end, the MEMS compliant mechanism is fabricated and measured to verify our analysis.

II. ADVANTAGE OF CURVED BEAM

Compliant mechanism relies on bending and deflection to achieve the designed function of specific deformation and movement. Combining topology optimization and a pseudo-rigid-body mode [12] in a structural topology design stage, an optimized multi-curved-beam structure can be generated to fulfill a specific movement. The geometry consideration of a multibeam structure has been discussed in detail in another publication [11]. The most important factor of curved beams in a compliance application is the ability to smoothen the structural profile, in order to avoid the stress concentration which happens at the edge or corner. Because the shape and the stress state of a compliant mechanism are changing during a large deflection, it is possible to distribute the stress and overcome the stress concentration by means of a curved-beam design. The objective of the simple example that is shown in Table I is to get a 42-μm output displacement in the Y-direction in a constrained design area. The curved beam shows a higher possibility to achieve the objective with a lower stress and an external force. Based on this concept, we design and fabricate the demonstrator device.

III. DEMONSTRATOR DEVICE

In this paper, an in-plane micro rotational mirror (see Fig. 1) is used as the demonstrator to explain the criterion idea. The dimension of the device is $2.2\ \text{mm} \times 2.6\ \text{mm} \times 150\ \mu\text{m}$, and the minimum beamwidth is 20 μm. The function of the 2-D rotational mirror is used to deliver a 34-μm linear input displacement from the load point and to transfer it to 10° of rotational movement with a fixed rotational center as the output at the mirror section. Most importantly, the structural device is constituted by only one component and relies on the compliance of SCS to achieve the function that we specified. The device is designed in two steps. In the first step, topology optimization is used to generate an initial structural layout. In the second step, computer-aided design (CAD) software is used to modify the structural topology in order to smoothen the profile and overcome stress problems. During the modification, a pseudo-rigid-body mode is used to analyze the kinematic

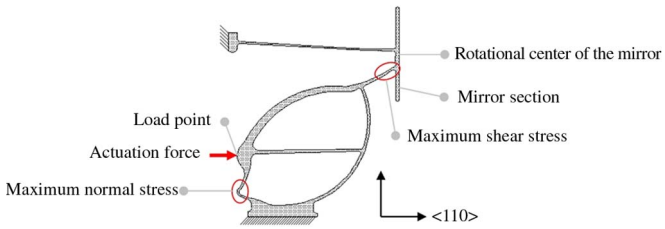

Fig. 1. Thin-curved-beam device obtained from the mechanism analysis with a pseudo-rigid-body model. The maximum shear stress occurs at the beam below the mirror section (upper right ellipse) and the maximum normal stress occurs at the meander, which is located below the load point (lower left ellipse). The minimum beamwidth is 20 μm, and the dimension of the device is 2.2 mm $\times$ 2.6 mm $\times$ 150 μm.

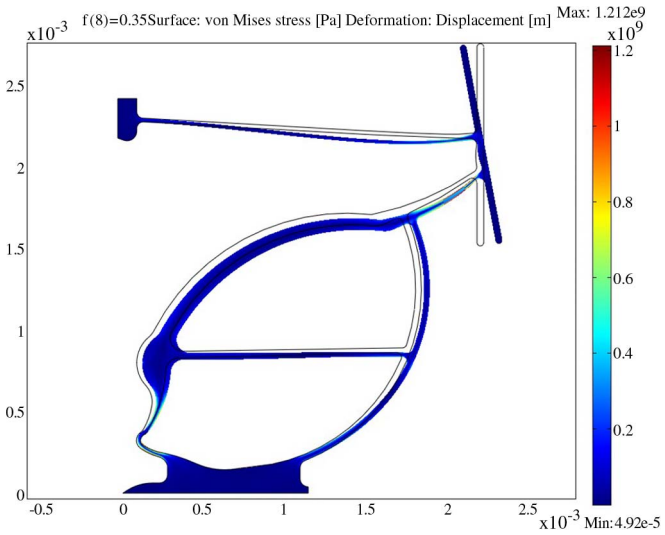

Fig. 2. Deformation and the stress state of the SCS compliant mechanism in a 2-D plane stress model.

motion. The relation between the geometry and the stress is analyzed by finite-element methods. The compliant mechanism is attached to a frame at two fixation lines (Fig. 1, top left and bottom). The input with a horizontal actuation force on the left generates a rotation through the center point of the mirror section on the right side; see Fig. 2. Based on the geometric design of this curved-beam device, which has been discussed in another paper [11], we extend the detailed discussion here on the directional properties of SCS device and its orientation layout consideration. In order to estimate the stress scale, we used the Young's modulus in the $\langle 110 \rangle$ orientation for a 2-D simulation [10]. We found that the maximum shear stress occurs at the beam below the mirror section (Fig. 1, upper right ellipse) and the maximum normal stress occurs at the meander below the load point (Fig. 1, lower left ellipse). By means of the 2-D simulation, we precisely analyze the stress state of different orientation layouts by 3-D simulation and fabricate the device by a standard silicon process.

IV. Layout Considerations

The general analysis of the stress scale and the deformation of a compliant mechanism can be easily estimated by 2-D

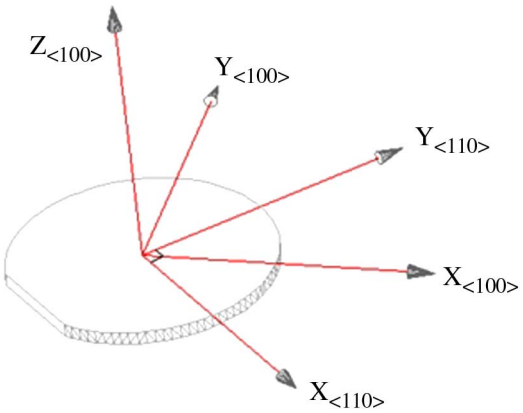

Fig. 3. Three main axes of the global coordinate system are defined as $X_{\langle 110 \rangle}$, $Y_{\langle 110 \rangle}$, $Z_{\langle 100 \rangle}$, and the three axes of the coordinate system of 45° coordinate plane rotation is defined as $X_{\langle 100 \rangle}$, $Y_{\langle 100 \rangle}$, $Z_{\langle 100 \rangle}$. The Z-axis is the rotational axis.

simulation. However, SCS is an anisotropic material. For a full description, it is necessary to use the theoretically corresponding stiffness matrix for a specific coordinate system and to understand the real stress state, displacement, and deformation of this device in a 3-D model [13]. First of all, we have to define the global coordinate system and make sure that the basic stiffness matrix is correct in order to calculate the specific stiffness matrices of different orientations in the wafer plane.

A. Stiffness Matrix

1) (100) Wafer: By using Young's modulus, shear modulus, and Poisson's ratio of the three main axes of a coordinate system, we can define a stiffness matrix by a generalized Hooke's law [9]. In our design, we use the primary flat [110] direction as the X-axis of the global coordinate system. Because the layout is on the wafer plane, [001] is used for (100) wafer as the Z-axis. The brackets we use in this paper follow the standard definition, for example, [100] represents a specific crystal direction and $\langle 100 \rangle$ represents the family of a crystal orientation. In order to explain more easily, the X-direction of the global coordinate system on a (100) wafer is defined as $X_{\langle 110 \rangle}$, the perpendicular Y-axis is defined as the $Y_{\langle 110 \rangle}$. The normal direction of the wafer plane is defined as the $Z_{\langle 100 \rangle}$, which is the rotational axis of layout coordinates; see Fig. 3. Under the coordinate system definition, the Young's moduli $E_1 = E_2 = E_{\langle 110 \rangle} = 168.9$ GPa and $E_3 = E_{\langle 100 \rangle} = 130$ GPa, and the shear moduli $G_{13} = 80$ GPa and $G_{12} = 51$ GPa are substituted to the stiffness matrix of the global coordinate system, and the value is as follows:

$$\begin{bmatrix} 195 & 36 & 64 & 0 & 0 & 0 \\ 36 & 195 & 64 & 0 & 0 & 0 \\ 64 & 64 & 166 & 0 & 0 & 0 \\ 0 & 0 & 0 & 80 & 0 & 0 \\ 0 & 0 & 0 & 0 & 80 & 0 \\ 0 & 0 & 0 & 0 & 0 & 51 \end{bmatrix} \text{(GPa)}. \quad (1)$$

Furthermore, by using the following transformation formulas [10], we can map the corresponding stiffness matrix from the

global coordinate system to arbitrary coordinate system in the (100) wafer plane:

$$C'_{11} = C_{11} + C_c\left(l_1^4 + m_1^4 + n_1^4 - 1\right) \tag{2}$$

$$C'_{12} = C_{12} + C_c\left(l_1^2 l_2^2 + m_1^2 m_2^2 + n_1^2 n_2^2\right) \tag{3}$$

$$C'_{13} = C_{13} + C_d\left(l_1^2 l_3^2 + m_1^2 m_3^2 + n_1^2 n_3^2\right) \tag{4}$$

$$C'_{33} = C_{33} + C_c\left(l_3^4 + m_3^4 + n_3^4 - 1\right) \tag{5}$$

$$C'_{44} = C_{44} + C_c\left(l_2^2 l_3^2 + m_2^2 m_3^2 + n_2^2 n_3^2\right) \tag{6}$$

$$C'_{66} = C_{66} + C_c\left(l_1^2 l_2^2 + m_1^2 m_2^2 + n_1^2 n_2^2\right) \tag{7}$$

$$C_c = C_{11} - C_{12} - 2C_{44} \tag{8}$$

$$C_d = C_{11} - C_{13} - 2C_{44} \tag{9}$$

$$\begin{vmatrix} l_1 & m_1 & n_1 \\ l_2 & m_2 & n_2 \\ l_3 & m_3 & n_3 \end{vmatrix} = \begin{vmatrix} \cos\theta & \sin\theta & 0 \\ -\sin\theta & \cos\theta & 0 \\ 0 & 0 & 1 \end{vmatrix} \tag{10}$$

where C_{ij} is the component of the stiffness matrix of the global coordinate system, C'_{ij} is the component of stiffness matrix of the rotated coordinate system, and l, m, and n are the components of the directional cosine. For example, the stiffness matrix of 12° rotation of coordinate ($X_{\langle 110\rangle - 12^\circ}$, $Y_{\langle 110\rangle - 12^\circ}$, $Z_{\langle 100\rangle}$; see Fig. 3) is as follows:

$$\begin{bmatrix} 180.5 & 49.5 & 64 & 0 & 0 & 0 \\ 49.5 & 180.5 & 64 & 0 & 0 & 0 \\ 64 & 64 & 166 & 0 & 0 & 0 \\ 0 & 0 & 0 & 80 & 0 & 0 \\ 0 & 0 & 0 & 0 & 80 & 0 \\ 0 & 0 & 0 & 0 & 0 & 65.5 \end{bmatrix} \text{(GPa)}. \tag{11}$$

The stiffness matrix shown in (11) will be used in the next section. In order to verify the correctness of this transformation, we separately calculate the stiffness matrix of the three-$\langle 100\rangle$ coordinate system ($X_{\langle 100\rangle}$, $Y_{\langle 100\rangle}$, $Z_{\langle 100\rangle}$) by using the generalized Hooke's law and by using the transformation formulas based on the global coordinates. Both of the values are the same and as follows [10]:

$$\begin{bmatrix} 166 & 64 & 64 & 0 & 0 & 0 \\ 64 & 166 & 64 & 0 & 0 & 0 \\ 64 & 64 & 166 & 0 & 0 & 0 \\ 0 & 0 & 0 & 80 & 0 & 0 \\ 0 & 0 & 0 & 0 & 80 & 0 \\ 0 & 0 & 0 & 0 & 0 & 80 \end{bmatrix} \text{(GPa)}. \tag{12}$$

Because of the verification, we make sure that the value of stiffness matrices can be used to analyze the deformation and the stress state of the SCS device in 3-D simulation.

2) (111) Wafer: The (111) wafer plane is a close-packed plane, and the difference of driving force in each direction on the wafer plane can be ignored [14], [15]. If there is no any internal defect in the material, we can use only one stiffness matrix to describe the mechanical behavior of the wafer plane. In other words, we can use the same value for the X- and Y-axes to simplify the calculation. Based on this concept, the original engineering constants of the Y-axis $[11\bar{2}]$ of a (111) SCS wafer is replaced by the X-axis [110]. Therefore, using the same way as we have discussed in the global coordinate system of (100) wafers, the primary flat $\langle 110\rangle$ orientation is used to define the $X_{\langle 110\rangle}$ and the $Y_{\langle 110\rangle}$. The normal direction of the wafer plane [111] is defined as the $Z_{\langle 111\rangle}$. Under the coordinate system definition, the Young's moduli $E_1 = E_2 = E_{\langle 110\rangle} =$ 168.9 GPa and $E_3 = E_{\langle 111\rangle} = 187.5$ GPa are substituted to a generalized Hooke's law, and the stiffness matrix of the (111) wafer plane is shown in the following:

$$\begin{bmatrix} 191 & 57 & 45 & 0 & 0 & 0 \\ 57 & 191 & 45 & 0 & 0 & 0 \\ 45 & 45 & 204 & 0 & 0 & 0 \\ 0 & 0 & 0 & 58 & 0 & 0 \\ 0 & 0 & 0 & 0 & 58 & 0 \\ 0 & 0 & 0 & 0 & 0 & 67 \end{bmatrix} \text{(GPa)}. \tag{13}$$

B. Layout Orientation

The structural device we used in this paper is a multi-curved-beam compliant mechanism. Based on the displacement and the stress considerations, the specific positions among the beams construct the structural topology. The orientation of each beam is therefore related to each other. In this situation, the relation among the actuation, the maximum stress beam, and the coordinate system has to be analyzed in order to find a suitable orientation of the structure layout on a SCS wafer. Because the material properties of the SCS wafer are 45° symmetry on the (100) plane [10], normally, we only need to analyze the 45° region between $\langle 100\rangle$ and $\langle 110\rangle$ orientations and map the same properties to the whole wafer. However, our device is not a symmetric structure. We also need to analyze the different stress states between clockwise and anticlockwise movements in the global coordinate system.

In order to understand the influence of the orientation of this SCS structure on its kinematic motion and robustness, we define and compare six different orientation layouts on a (100) wafer and one layout on a (111) wafer. The seven layouts have different coordinate systems, which are shown in Fig. 4. The tilt of the maximum shear stress beam [(MSB); below the mirror; see Fig. 1] is 33° away from the direction of the actuation force, which is defined to align with the X-direction of the specific coordinate system. Because of the tilt of this beam, we choose 12° as a distinction to define each layout and discuss the relation between the rotation of coordinate systems and orientation layouts.

In (100) wafer, the structure of layout (1) is in the global coordinate system, and the orientation of the MSB is 12° away from $\langle 100\rangle$ orientation and 33° away from $\langle 110\rangle$ orientation. In layout (2), the MSB aligns to $\langle 100\rangle$ orientation, and the actuation force (or the coordinate system) is anticlockwise 12° away from $\langle 110\rangle$ orientation. In layout (3), the orientation of the MSB is pointing to the center of $\langle 100\rangle$ and $\langle 110\rangle$, in other words, 22.5° away from $\langle 110\rangle$ orientation. Aside from layouts (2), (3), and (5), all other layouts are based on the same rule subsequently to show a 12° angle between the MSB and either the $\langle 100\rangle$ or $\langle 110\rangle$ orientation, in order to cover and conclude

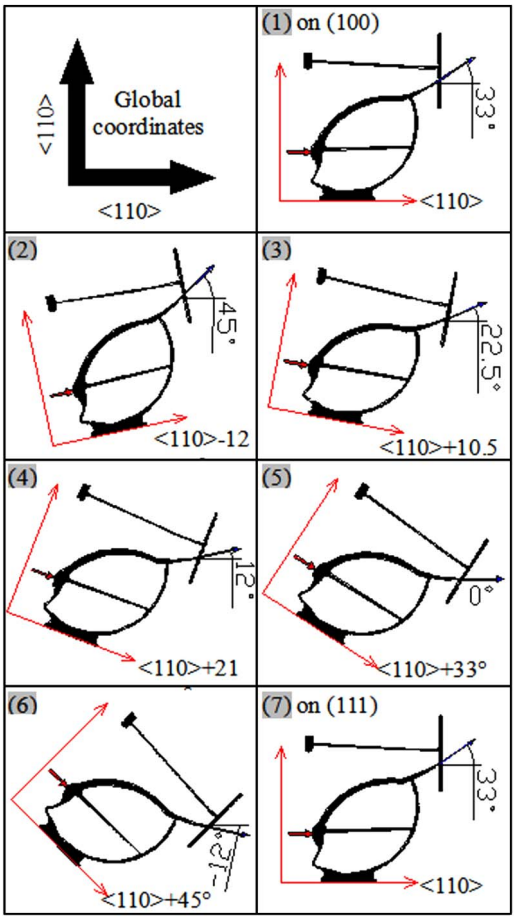

Fig. 4. Seven orientation layouts and defined coordinate systems on SCS wafer. The angle between the MSB and the X-axis is 33°. Layouts (1) and (7) are aligned to the global coordinate system.

the different behavior of the structure between $\langle 110\rangle - 45°$ and $\langle 110\rangle + 12°$, from anticlockwise to clockwise. In (111) wafer, the structure of layout (7) aligns again to the global coordinate system.

In the next step, Comsol [13] is used to simulate the deformation and analyze the stress of this structure. With a rough 2-D plane stress analysis, we found that the maximum stress (von Mises) of the structure is about 1.2 GPa (see Fig. 2), which reaches the fracture strength of SCS [16], when the mirror section of the device rotates about 12°. Because the maximum stress must be maintained below the fracture strength of the material, we define 10° rotational angle of the mirror as the limit. In the precise 3-D simulation, the aforementioned seven layouts with the corresponding stiffness matrices are compared and analyzed. Because the 3-D mesh densities of the seven layouts have to be unified, there is only one CAD model, which is constructed of quadratic quadrilateral mesh; see Fig. 5. The corresponding stiffness matrices were used in the calculation of each orientation layout. From the simulation results, we find that the input displacement for 10° rotational angle of the mirror is 34 μm, and it is the same in the seven orientation layouts. The differences are in the actuation force and in the stress state, because of the directional Young's modulus of SCS. The coordinate system of a layout closer to the global coordinate system needs a larger actuation force, and vice versa; see Fig. 6.

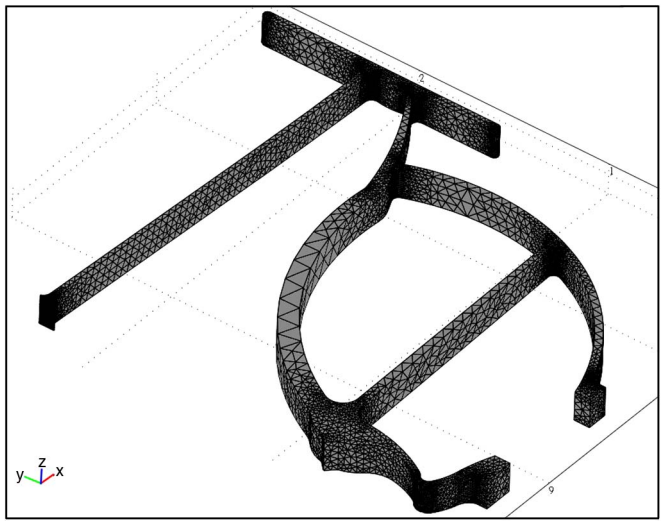

Fig. 5. Three-dimensional structural model of the SCS device, which is constructed of quadratic quadrilateral meshes.

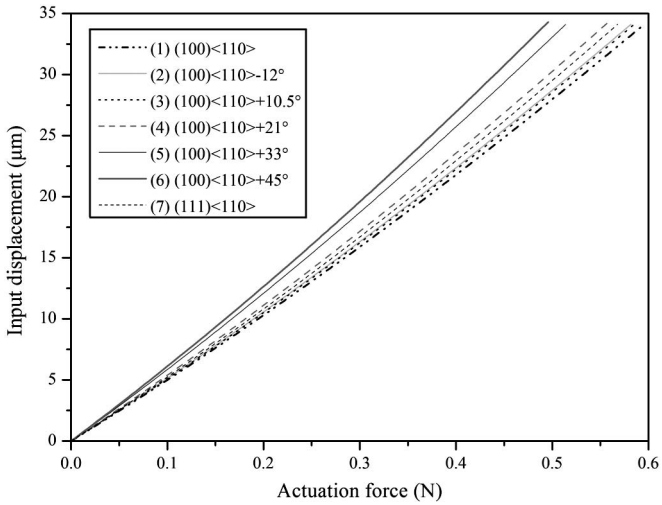

Fig. 6. Relation between input displacement and the actuation force. The device located on the seven orientation layouts has the same input displacement (34 μm) for achieving 10° of rotational angle in the mirror section. Nevertheless, the corresponding actuation forces are different.

C. Orientation Map

The compliant mechanism uses bending to achieve hinge function; in other words, the rotational angle of the mirror section is the required function of the device. When the device is driven by an actuator, the stress state of the compliant mechanism is complicated, since each point along a curved beam has a different effective cross-sectional elastic property. However, from the analysis of the data, we find that there are two key factors for a design criterion. The first one is the orientation of the MSB. The second one is the orientation of the connection line between the point of the maximum shear stress (at the bottom of MSB) and the point of the minimum stress (on the top of MSB). We define this connection line as MSL; see Fig. 7. The bending moment on MSB is represented by a pair of curved arrows.

The bending of MSB is unsymmetrical, which means that the ultimate shear stress may not be stationary. In reality, during

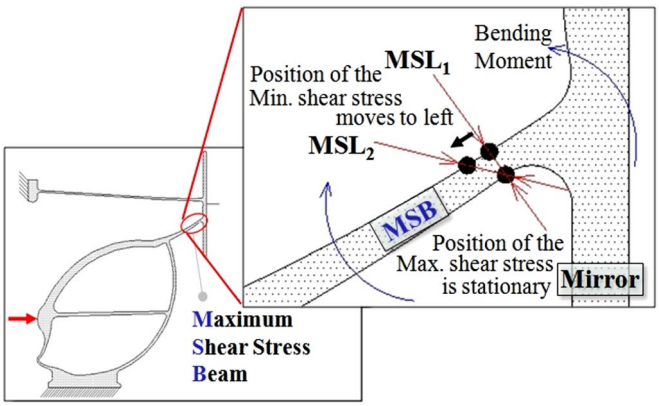

Fig. 7. Definitions of MSB and MSL at the maximum shear stress region of the structure. During the actuation, the position of the maximum shear stress is stationary. However, the position of the minimum shear stress moves forward to the left, when the critical stress is reached. Therefore, the orientation of MSL is changed.

the bending, there is a critical threshold stress. When the stress exceeds the critical threshold stress, the position of the ultimate stress would change. In our case, the point of the minimum shear stress moves forward to the left, when the stress reaches the critical threshold stress. Hence, we simulate the force-displacement behavior of the mirror structure to find the critical stress, and simultaneously, the corresponding orientations of MSL_1 (before) and MSL_2 (after).

Because it is easier to explain it by the rotational angle of the mirror section, the critical angle of the mirror is used to replace the critical stress. Fig. 8 shows each layout (a) below and (b) above its critical angle. The angle in the box inset indicates the critical tilting angle of the mirror when MSL starts to tilt toward the left ($MSL_1 \rightarrow MSL_2$). The angle between MSL and the [110] direction is shown by the bent arrow. The turning of MSL is obvious for each case; we rearrange the data and categorize the seven layouts as three types (see Table II).

1) The orientations of both MSB and MSL are close to $\langle 110 \rangle$. Layouts (5) and (6) correspond to this type. Because of the high possibility to cause a crystal slip in the whole region (0°–11°), it is better to avoid this kind of layout.
2) The orientation of MSB is far away from $\langle 110 \rangle$, but the orientation of MSL is close to $\langle 110 \rangle$. Layout (2) corresponds to this type. When the angle rotates more than 5°, the possibility to induce a crystal slip would be increased. This kind of orientation layout is only suitable for small deflection.
3) The orientation of MSL is far away from $\langle 110 \rangle$. Layouts (1), (3), (4), and (7) correspond to this type. Between 12° and 33° of MSB orientation, it can efficiently decrease the possibility of slip.

Based on the three types, we find a "21 ° safe region." If the orientation layout of MSB can avoid the 12° region that deviate from both $\langle 100 \rangle$ and $\langle 110 \rangle$, the SCS compliant mechanism can efficiently decrease the crystal slip and efficiently use its elasticity to achieve a large deformation.

Due to the symmetry of (100) SCS wafer, we can thus plot a map of safe layout orientation, which directly illustrates the

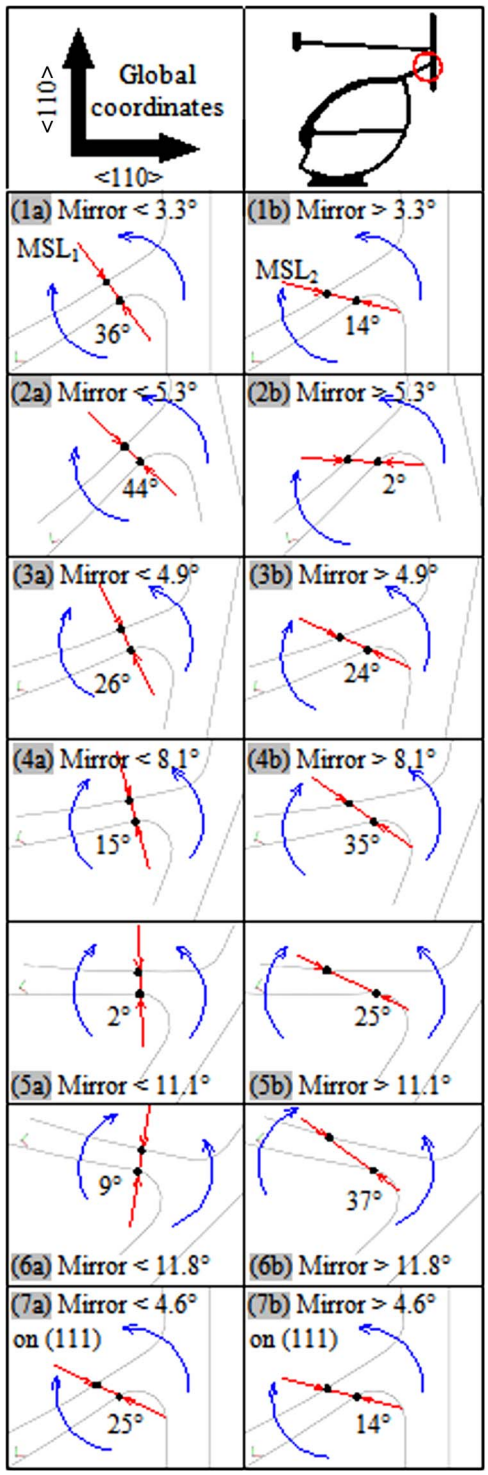

Fig. 8. Stress states and deviations of the seven orientation layouts. During kinematic motion, the maximum stress beam is under unsymmetrical bending. When the rotational angle of the mirror exceeds the critical angle, the tilting direction of MSL is changed.

safe regions and those which should be avoided; see Fig. 9. Meanwhile, from the analysis of layout (7) for (111) wafer, we find that there is no obvious slip mechanism. Nevertheless, a scratch, which is located at the sidewall of the maximum stress beam, would be an initial failure source to induce a crack [17] and then transmit to align with $\langle 110 \rangle$ orientation. Under

TABLE II
THREE TYPES OF ORIENTATION LAYOUT ARE DEFINED AFTER CLASSIFICATION. TYPE 1 IS NOT A GOOD ORIENTATION LAYOUT. TYPE 2 IS ONLY SUITABLE FOR GENERAL APPLICATIONS WITH SMALL DEFLECTION. TYPE 3 IS SUITABLE FOR LARGE DEFLECTION APPLICATION AS FOR THE COMPLIANT MECHANISM TREATED IN THIS PAPER

	Layout	X-axis of coordinate	Orientation of MSB	Orientation of MSL		Critical shear stresses (GPa)	Criterion
Type 1	(5)	<110>+33°	<110>	Mirror < 11.1°	Mirror > 11.1°	Min. -0.63 Max. 0.75	-
				<110>+2°	<110>+25°		
	(6)	<110>+45°	<110>-12°	Mirror < 11.8°	Mirror > 11.8°	Min. -0.65 Max. 0.78	
				<110>+9°	<110>+37°		
Type 2	(2)	<110>-12°	<110>+45°	Mirror < 5.3°	Mirror > 5.3°	Min. -0.21 Max. 0.25	O
				<110>+44°	<110>+2°		
Type 3	(1)	<110> on (100) wafer	<110>+33°	Mirror < 3.3°	Mirror > 3.3°	Min. -0.33 Max. 0.39	+
				<110>+36°	<110>+14°		
	(3)	<110>+10.5°	<110>+22.5°	Mirror < 4.9°	Mirror > 4.9°	Min. -0.3 Max. 0.36	
				<110>+26°	<110>+24°		
	(4)	<110>+21°	<110>+12°	Mirror < 8.1°	Mirror > 8.1°	Min. -0.49 Max. 0.58	
				<110>+15°	<110>+35°		
	(7)	<110> on (111) wafer	<110>+33°	Mirror < 4.6°	Mirror > 4.6°	Min. -0.26 Max. 0.3	
				<110>+25°	<110>+14°		

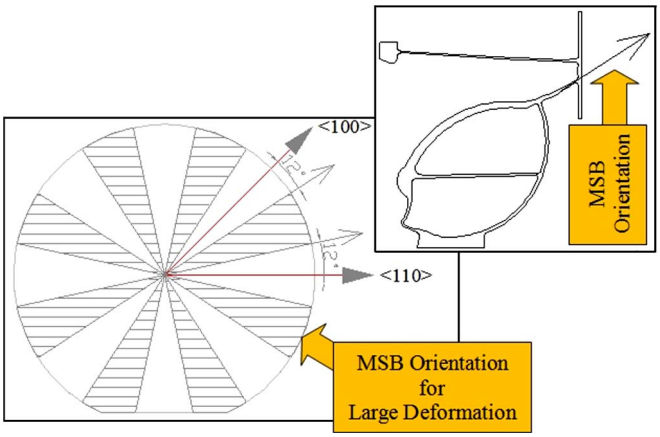

Fig. 9. Shaded regions are the safe layout orientations of the MSB on a (100) wafer.

a conservative consideration, it is also better to follow this orientation map in order to maintain the robustness.

V. EXPERIMENTAL VERIFICATION

In order to verify the simulation result, some demonstrator devices were arranged on SCS wafers by following the three types of orientation layout that had been summed up in Table II. After that, those thin-beam structures were shaped by an inductively coupled plasma dry etching. The etching parameters follow the standard deep etching recipe [18]. Six samples for each type on (100) wafer and three samples on (111) wafer were prepared and pushed by a piezoelectric actuator. The experimental result is shown in Table III.

From the experimental result of those devices which are fabricated on (100) wafers, we find that the variance of the stable maximum rotational angle is large, which is from 2° to 11.5°. Those specimens that can reach stable 10° rotational angle belong to type 3 in which the corresponding input displacement is 33–35 μm; see Figs. 10 and 11. The failure possibility of other specimens from types 1 and 2 is higher in the first 10–20 μm input range, and the average rotational angles are 3° and 4° separately. In addition, the rotational angle of those specimens which are fabricated on (111) wafers is between 8° and 9.5°.

TABLE III
EXPERIMENTAL RESULTS OF THE ROTATIONAL ANGLES OF THE MIRROR SECTION. THE MEASUREMENT TOLERANCE OF THE ANGLE IS ±0.5°

	Max. rotational angle	Min. rotational angle	Average rotational angle
Type 1	4°	2°	3°
Type 2	5°	2°	4°
Type 3 (100) wafer	11.5°	7°	9°
Type3 (111) wafer	9.5°	8°	8.5°

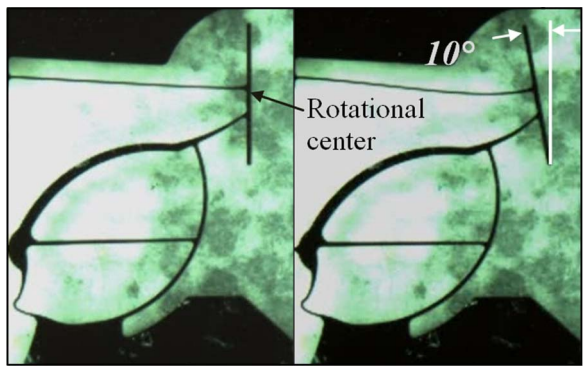

Fig. 10. Optical micrograph shows 10° of rotational angle with a stationary rotational center. The compliant micro rotational mirror is made of SCS with the dimension 2.2 mm × 2.6 mm × 150 μm. The corresponding input displacement is 33–35 μm.

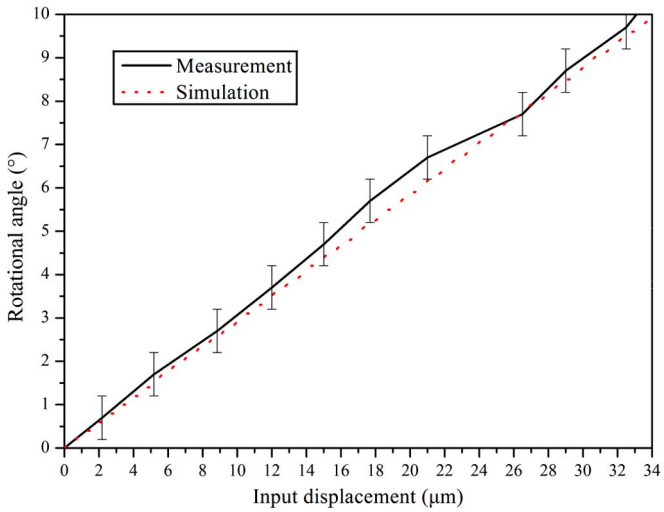

Fig. 11. Comparison between the simulation and a measurement result shows that both corresponding input displacements for a 10° rotational angle are 34 μm.

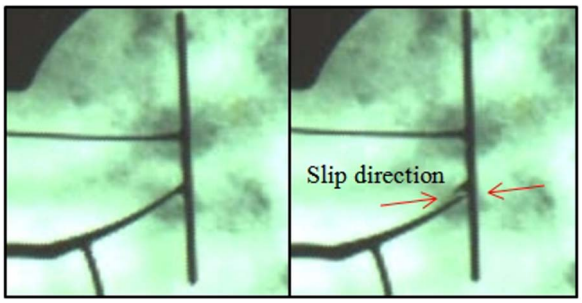

Fig. 12. Close-up view of a crystal slip on MSB. The slip direction is close to the $\langle 110 \rangle$ orientation, which is the main failure mechanism of type 1, and the corresponding rotational angle is less than 5°.

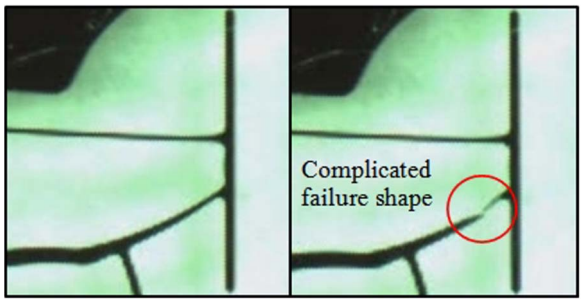

Fig. 13. Close-up view of the breakage on MSB. The breakage shape is more complicated, and a small section of the beam is separated and disappeared. The fracture strength dominates the failure of type 3.

Observing under an optical micrograph, the failure shape of types 1 and 2 is mostly straight and close to (110) orientation, and the corresponding rotational angle is less than 4°; see Fig. 12(b). In this kind of situation, the crystal slip is a main failure mechanism. On the other hand, the fracture that happens in a large deflection has a more complicated shape, and a small section of the beam is separated and disappeared; see Fig. 13(b). The fracture strength can be trusted, and the Young's modulus can be exploited in this kind of situation. Both of the two measured results are the same as the analysis in the simulation.

VI. Conclusion

Based on the theories of elasticity and numerical analysis method, we successfully fabricated a compliant mechanism device which can generate specific movement with multi-curved-beams. Our analysis method can be generalized as follows.

1) Analyze the deformation and the stress state with corresponding stiffness matrices in simulation software.
2) Find the MSB of the device.
3) Find the positions of ultimate shear stresses, and connect the two points of ultimate stresses as a line (MSL).
4) Calculate the angle between MSL and the slip direction $\langle 110 \rangle$ of SCS.
5) Decide the suitable orientation of the device on the SCS wafer in order to avoid crystal slip.

By using this design rule, we have demonstrated that this fabricated device has the same behavior as predicted in analysis and simulation. The micro rotational mirror can reach 10° of rotational angle through 34 μm of input displacement and achieves large deflection with a brittle material. In order to decrease the possibility of failure, choosing a suitable coordinate frame to balance the actuation force, stiffness, and the orientation of the maximum stress beam of the device is a key step. The general criterion for the layout of a bending beam is to avoid the occurrence that the connection line between the maximum shear stress point and the minimum stress point is parallel or close to the $\langle 110 \rangle$ orientations. Furthermore, for a large deflection application on (100) wafers, the maximum stress beam shall deviate 12 °–33° from $\langle 110 \rangle$ orientation. For the orientation layout on a (111) wafer, it is better to arrange the orientation of MSL far away from the $\langle 110 \rangle$ orientation to decrease the possibility of initial cracks generated in the slip direction. In other words, if crystal slip and the initial cracks can be avoided or reduced, the fracture strength of SCS can be a reliable index to predict the maximum rotational angle of the rotational mirror. Moreover, an SCS compliant mechanism can exploit on its high Young's modulus to achieve a large deflection, if the device is fabricated by correct orientation layouts and the maximum intrinsic stress is maintained below the elastic limit.

References

[1] S. Kota, J. Joo, Z. Li, S. M. Rodgers, and J. Sniegowski, "Design of compliant mechanisms: Applications to MEMS," *Analog Integr. Circuits Signal Process.*, vol. 29, no. 1/2, pp. 7–15, Oct. 2001.
[2] M. P. Bendse and O. Sigmund, *Topology Optimization*, 2nd ed. Berlin, Germany: Springer-Verlag, 2003, pp. 94–95.
[3] H. Maddisetty and M. Frecker, "Dynamic topology optimization of compliant mechanisms and piezoceramic actuators," *ASME J. Mech. Des.*, vol. 126, no. 6, pp. 975–983, Nov. 2004.
[4] F. Lotti, P. Tiezzi, G. Vassura, and A. Zucchelli, "Mechanical structures for robotic hands based on the 'compliant mechanism' concept," in *Proc. 7th ESA Workshop Adv. Space Technol. Robot. Autom.*, Noordwijk, Netherlands, 2002, section 2.7b-1, pp. 1–8.
[5] A. C. Ugural, *Mechanical Design: An Integrated Approach*. Boston, MA: McGraw-Hill, 2003, pp. 682–688.
[6] R. E. Reed-Hill and R. Abbaschian, *Physical Metallurgy Principles*, 3rd ed. Boston, MA: PWS-Kent, 1991, pp. 136–139.
[7] P. B. Hirsch, S. G. Roberts, and J. Samuels, "The brittle–ductile transition in silicon. II. Interpretation," in *Proc. R. Soc. Lond. A, Math. Phys. Sci.*, Jan. 1989, vol. 421, no. 1860, pp. 25–53.

[8] J. Turley and G. Sines, "The anisotropy of Young's modulus, shear modulus and Poisson's ratio in cubic materials," *J. Phys. D, Appl. Phys.*, vol. 4, no. 2, pp. 264–271, Feb. 1971.
[9] A. P. Boresi and K. P. Chong, *Elasticity in Engineering Mechanics*, 2nd ed. New York: Wiley, 2000, pp. 233–239.
[10] J. J. Wortman and R. A. Evans, "Young's modulus, shear modulus and Poisson's ratio in silicon and germanium," *J. Appl. Phys.*, vol. 36, no. 1, pp. 153–156, Jan. 1965.
[11] T. Chen, Z. Liu, J. G. Korvink, S. Krausse, and U. Wallrabe, "Topology optimization for micro rotational mirror design and safe manufacturing," in *Proc. 22nd Int. Conf. Micro Electro Mech. Syst.*, 2009, pp. 1019–1022.
[12] L. L. Howell, *Compliant Mechanisms*. New York: Wiley, 2001, pp. 38–40.
[13] *Comsol 3.3, Structural Mechanics Module User's Guide*, Comsol AB, Stockholm, Sweden, 2006, pp. 324–363.
[14] J. Kim, D.-I. Cho, and R. S. Muller, "Why is (111) silicon a better mechanical material for MEMS," in *Proc. Transducers Conf.*, 2001, pp. 662–665.
[15] O. M. Jadaan, N. N. Nemeth, J. Bagdahn, and W. N. Sharpe, "Probabilistic Weibull behavior and mechanical properties of MEMS brittle materials," *J. Mater. Sci.*, vol. 38, no. 20, pp. 4087–4113, Oct. 2003.
[16] K. Petersen, "Silicon as a mechanical material," *Proc. IEEE*, vol. 70, no. 5, pp. 420–457, May 1982.
[17] J. Bagdahn, W. N. Sharpe, and O. Jadaan, "Fracture strength of polysilicon at stress concentrations," *J. Microelectromech. Syst.*, vol. 12, no. 3, pp. 302–312, Jun. 2003.
[18] H. Ashraf, J. K. Bhardwaj, S. Hall, J. Hopkins, A. M. Hynes, I. Johnston, S. McAuley, G. Nicholls, L. Atabo, M. E. Ryan, and S. C. Watcham, "Advances in deep anisotropic silicon etch processing for MEMS," in *Proc. 5th Italian Conf. Sens. Microsyst.*, 2000, pp. 322–329.

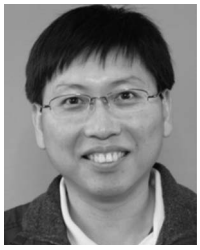

Tzung-Ming Chen received the Ph.D. degree in microsystems engineering from the Department of Microsystems Engineering, University of Freiburg, Freiburg, Germany, in 2009, with a scholarship offered by the Ministry of Education of Taiwan.

Since August 2009, he has been with the Department of Mechanical Engineering, Army Academy, Jhongli City, Taiwan, continuing his research. His research focuses on the design and analysis of microcompliant mechanisms and fabrication procedures of high-aspect-ratio and multi-curved-beam MEMS components.

Zhenyu Liu received the Ph.D. degree in mechanical engineering from Dalian University of Technology, Dalian, China, in 2000.

From 2001 to 2008, he was a Research Assistant and a Group Leader in the Department of Microsystems Engineering, University of Freiburg, Freiburg, Germany. Since 2009, he has been with Changchun Institute of Optics, Fine Mechanics and Physics, Chinese Academy of Sciences, Changchun, China. His research interests are the simulation and optimization of devices in MEMS.

Jan G. Korvink received the M.Sc. degree in computational mechanics from the University of Cape Town, Cape Town, South Africa, in 1987, and the Ph.D. degree in applied computer science from the Swiss Federal Institute of Technology (ETH) Zurich, Zurich, Switzerland, in 1993.

Following his graduate studies, he joined the Physical Electronics Laboratory, ETH Zurich, where he established and led the MEMS Modeling Group. This was followed by a move in 1997 to the University of Freiburg, Freiburg, Germany, where he is currently a Professor of microsystems engineering, runs the Laboratory for Microsystem Simulation, and is the Director of the School for Soft Matter Research, Freiburg Institute for Advanced Studies. He has written more than 180 journal and conference papers in the area of microsystem technology and coedits the review journal *Applied Micro and Nanosystems* (see http://www.wiley-vch.de/books/info/amn). His research interests include modeling and simulation, and low-cost fabrication of microsystems.

Ulrike Wallrabe received the Diplom degree in physics from the University of Karlsruhe, Karlsruhe, Germany, and the Ph.D. degree in mechanical engineering of microturbines and micromotors from the Department of Mechanical Engineering, University of Karlsruhe, Karlsruhe, in 1992.

From 1989 to 2003, she was with the Institute for Microstructure Technology, Forschungszentrum Karlsruhe, Karlsruhe, where she focused on microactuators and optical MEMS made by the LIGA technique. Since 2003, she has been a Professor of microactuators in the Department of Microsystems Engineering, University of Freiburg, Freiburg, Germany. She currently holds a fellowship at the Freiburg Institute of Advanced Studies, University of Freiburg. She has published more than 90 papers in the field of microsystems technology. Her focus is on magnetic microstructures, microcoils, and adaptive optics.